Relaxation time of the global order parameter on multiplex networks: The role of interlayer coupling in Kuramoto oscillators

Alfonso Allen-Perkins,[1,2,*] Thiago Albuquerque de Assis,[1,2,†] Juan Manuel Pastor,[1,‡] and Roberto F. S. Andrade[2,§]

[1]*Complex System Group, Universidad Politécnica de Madrid, 28040-Madrid, Spain*

[2]*Instituto de Física, Universidade Federal da Bahia, 40210-210 Salvador, Brazil*

(Received 3 August 2017; revised manuscript received 10 October 2017; published 31 October 2017)

This work considers the time scales associated with the global order parameter and the interlayer synchronization of coupled Kuramoto oscillators on multiplexes. For two-layer multiplexes with an initially high degree of synchronization in each layer, the difference between the average phases in each layer is analyzed from two different perspectives: the spectral analysis and the nonlinear Kuramoto model. Both viewpoints confirm that the prior time scales are inversely proportional to the interlayer coupling strength. Thus, increasing the interlayer coupling always shortens the transient regimes of both the global order parameter and the interlayer synchronization. Surprisingly, the analytical results show that the convergence of the global order parameter is faster than the interlayer synchronization, and the latter is generally faster than the global synchronization of the multiplex. The formalism also outlines the effects of frequencies on the difference between the average phases of each layer, and it identifies the conditions for an oscillatory behavior. Computer simulations are in fairly good agreement with the analytical findings, and they reveal that the time scale of the global order parameter is half the size of the time scale of the multiplex, if not smaller.

DOI: 10.1103/PhysRevE.96.042312

I. INTRODUCTION

The large number of recent investigations on multilayer networks have contributed to uncovering several topological and dynamical aspects of complex systems [1–6]. These studies have been motivated by the observation that several such systems can be been divided, in a very natural way, into subsets of components that interact in a different way with the coparticipants of the same set as compared to members of other subsets. In this way, each such subset can be represented by a layer of a multilayer network. This concept has proven to be broad enough to represent different interaction aspects of the same agent, provided it also interacts differently with members of other subsets [7–9].

Multiplexes form a particular class of multilayer networks, where each layer is formed by the same number N of nodes. Moreover, a multiplex is formed by agents that are identified as one network node, with its own label, in every multiplex layer [9–11]. Because of this, each of these agent's representation is connected to its own representations in all other layers [12–14]. The strength of these interactions can be dependent of the agent and of the layers between which the interaction occurs [15–17].

These properties make multiplexes a suitable representation of actual complex systems, where each agent has multiple purposes and abilities. This is the case, for instance, for economic systems in which each agent represents an investor that can trade in different world markets. It can use the communication flow between markets and different market features expressed by local bylaw restrictions to develop strategies in each market to maximize hedge, risk, and profits. Under these circumstances, it is natural to ask how and if cooperation and competition [18–23] favor the spread of information and synchronization [24–29] among the different layers, or the emergence of collective behavior such as self-organization [30,31] or epidemics [32].

To help understand real-world complex dynamics, several synchronous models with nonidentical interacting agents have been introduced for a description of synchronization, starting from the Rössler and Kuramoto models [33,34] in homogeneous structures. More recently, network science explored similar models on nonhomogeneous structures [25,35–37]. These dynamic models are sufficiently complex to be nontrivial and display a large variety of synchronization patterns. In particular, the Kuramoto model has the advantage of being sufficiently flexible that it can be adapted to many different contexts, and, at the same time, simple enough to be mathematically tractable [38]. Most of the research done on the Kuramoto model in complex networks has been summarized in the review of Rodrigues *et al.* [39].

The collective dynamics of several interacting populations of Kuramoto oscillators has been investigated on multilayers [40–42]. Most of the studies on network synchronization focus on the effects of network topology on the dynamics in the stationary regime, or when the asymptotic phase of the synchronization is reached. Other investigations have addressed the question of multiplex diffusion [5,43], and the limits to which it can be enhanced in comparison to the corresponding spread processes in a single layer. However, because the question of how fast the network synchronizes in the steady state is equally important [39], we want to focus here on the difference between diffusion and synchronization speed in multiplexes. The two phenomena are certainly related, but, as we will discuss in the forthcoming sections, they also present different features in multiplex topology.

In this work, we present analytical results for the multiplex order parameter derived from Kuramoto's equations of motion, both in the linear approximation and in their complete nonlinear form, under the assumption that the initial order

*alfonso.allen@hotmail.com

†thiagoaa@ufba.br

‡juanmanuel.pastor@upm.es

§randrade@ufba.br

 ©2017 American Physical Society

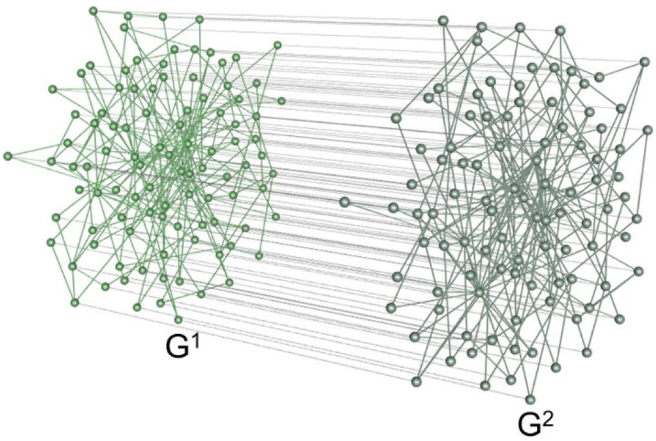

FIG. 1. Example of an undirected multiplex network with two layers, G^1 and G^2 (data visualization with MUXVIZ [44]).

parameter of each layer is close to unity. Numerical integration of the equations of motion corroborates these predictions and presents a consistent scenario in which it is possible to identify the diffusion relaxation time and the interlayer synchronization phase. As a consequence, the interlayer synchronization is observed to proceed at a faster or equal pace as compared to diffusion.

The paper is organized as follows. In Sec. II, we define the model and briefly list the main results of the diffusion relaxation time in multiplexes [1,2,5,43,45]. In Sec. III, the relaxation time of the order parameter and that of the interlayer synchronization are deduced from spectral analysis and the nonlinear Kuramoto model. Numerical results supporting the analytical expressions are presented in Sec. IV. Section V summarizes our conclusions.

II. KURAMOTO MODEL IN MULTIPLEXES AND DIFFUSION

We consider initially an undirected multiplex $\mathcal{M}$ with M layers G^α, $1 \leqslant \alpha \leqslant M$, where each layer contains N nodes identified by x_n^α, $1 \leqslant n \leqslant N$ (see Fig. 1). A system of coupled Kuramoto oscillators, which takes into account the intralayer and interlayer connections, is defined on $\mathcal{M}$. The oscillator in each node x_n^α of the layer G^α is characterized by its phase θ_n^α, whose dynamics is described by

$$\dot{\theta}_n^\alpha = \Omega_n^\alpha + \lambda^\alpha \sum_{x_m^\alpha \in G^\alpha} w_{nm}^\alpha \sin\left(\theta_m^\alpha - \theta_n^\alpha\right) + \sum_{\substack{\beta=1 \\ \alpha\neq\beta}}^{M} \lambda^{\alpha\beta} w_{nn}^{\alpha\beta} \sin\left(\theta_n^\beta - \theta_n^\alpha\right). \quad (1)$$

Here, Ω_n^α is the natural frequency of the oscillator x_n^α, λ^α and $\lambda^{\alpha\beta}$ are the coupling strength of the layer α and of the interlayer $\alpha\beta$, respectively, w_{nm}^α is the weight of the connection between the nodes x_n^α and x_m^α, and $w_{nn}^{\alpha\beta}$ is the weight of the connection between the nodes x_n^α and x_n^β. In the case of an unweighted and undirected $\mathcal{M}$, $w_{mn}^{\alpha\beta} = 1$ and $w_{nm}^\alpha = 1$ if there is a link between the nodes x_n^α and x_m^α, and 0 otherwise.

To present a closer comparison between the results for Eq. (1) and those for multiplex diffusion [1,2,5,43,46,47], we consider first the simplest case of an undirect $M = 2$ multiplex, without sources and sinks of frequency ($\Omega_n^\alpha = 0$), for which the linear approximation of the Kuramoto model reads

$$\dot{\theta}_n^\alpha(t) = \lambda^\alpha \sum_{x_m^\alpha \in G^\alpha} w_{nm}^\alpha \left(\theta_m^\alpha - \theta_n^\alpha\right) + \lambda^{12}\left(\theta_n^\beta - \theta_n^\alpha\right), \quad (2)$$

with $1 \leqslant n,\, m \leqslant N$, $1 \leqslant \alpha,\beta \leqslant 2$, and $w_{nn}^{12} = 1$.

Once Eq. (2) is equivalent to the multiplex diffusion equation [1,43], it can be written as

$$\dot{\vec{\theta}} = -\mathcal{L}\vec{\theta}, \quad (3)$$

where $\vec{\theta}$ is a column vector that describes the phase of the oscillators such that $\vec{\theta}^T = (\theta_1^1, \dots, \theta_N^1 | \theta_1^2, \dots, \theta_N^2)$, and X^T stands for the transpose of matrix X. $\mathcal{L}$, the *supra-Laplacian matrix* of $\mathcal{M}$, is defined as

$$\mathcal{L} = \left(\begin{array}{c|c} \lambda^1 \mathbf{L}_1 + \lambda^{12}\mathbf{I} & -\lambda^{12}\mathbf{I} \\ \hline -\lambda^{12}\mathbf{I} & \lambda^2 \mathbf{L}_2 + \lambda^{12}\mathbf{I} \end{array}\right), \quad (4)$$

where $\mathbf{I}$ is an $N \times N$ identity matrix and $\mathbf{L}_\alpha$ is the usual $N \times N$ Laplacian matrix of G^α, with elements $(\mathbf{L}_\alpha)_{nm} = s_n^\alpha \delta_{nm} - w_{nm}^\alpha$. $s_n^\alpha = \sum_{x_m^\alpha \in G^\alpha} w_{nm}^\alpha$ and δ is the Kronecker delta function.

To characterize the eigenvalue spectrum $S(\mathcal{L}) \equiv \{\Lambda_i\}$, we rank its eigenvalues in ascending order, $0 = \Lambda_1 < \Lambda_2 \leqslant \cdots \leqslant \Lambda_{2N}$ [43,48,49]. The solution of Eq. (3) in terms of the normal modes $\varphi_i(t)$ is given by

$$\vec{\varphi} = \mathbf{B}^T \vec{\theta}, \quad (5)$$

where $\varphi_i(t) = \varphi_i(0) e^{-\Lambda_i t}$, and $\mathbf{B} = (\vec{v}_1 | \vec{v}_2 | \cdots | \vec{v}_{2N})$ is the matrix of eigenvectors of $\mathcal{L}$ (i.e., $\Lambda_i \vec{v}_i = \mathcal{L}\vec{v}_i$) [43,48,49].

Consequently, the diffusive relaxation time of multiplex networks, $\tau_\mathcal{M}$, depends on the network topology and is dominated by the smallest nonzero eigenvalue Λ_2 of the $\mathcal{L}$, i.e., $\tau_\mathcal{M} = 1/\Lambda_2$ [5,43,45]. This behavior is in line with analogous findings for monolayer networks of coupled Kuramoto oscillators, which have shown that the relaxation time mainly depends on the smallest nonzero eigenvalue of the corresponding Laplacian matrix [50–53].

If we consider $\lambda^1 = \lambda^2 = 1$, the analytical results in Refs. [5,43] for multiplex diffusion indicate the following properties of $S(\mathcal{L})$:

(i) $2\lambda^{12} \equiv \Lambda_\Delta$ is always an eigenvalue of $\mathcal{L}$.

(ii) When the interlayer coupling is small, i.e., $\lambda^{12} \ll 1$, $\Lambda_2 = \Lambda_\Delta$.

(iii) When the interlayer coupling is large, i.e., $\lambda^{12} \gg 1$, $\Lambda_2 \sim \sigma_s/2$, where σ_s is the smallest nonzero eigenvalue of the superposition matrix $(L_1 + L_2)/2$, and L_α is the Laplacian matrix of layer α.

In Fig. 2 we show an example of the dependence of Λ_2 on λ^{12}.

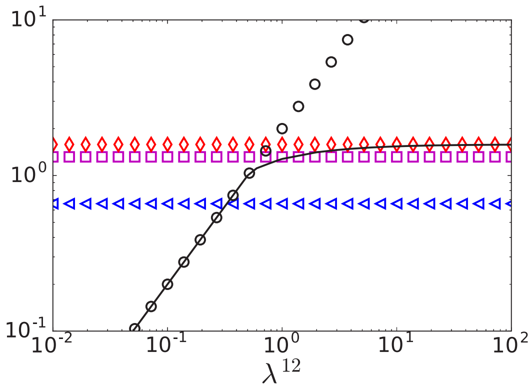

FIG. 2. Dependence on λ^{12} of the smallest nonzero eigenvalue σ_2 of the Laplacian matrices of layer 1 (blue triangles), layer 2 (magenta squares), the superposition of both layers (red rhombus), Λ_Δ (black circles), and Λ_2 (black continuous line). The results are presented for an $M = 2$ multiplex $\mathcal{M}$ with $N = 100$ nodes in each layer, when $\lambda^1 = \lambda^2 = 1$. Each layer consists of a scale-free network with degree distribution $P(k) \sim k^{-3}$.

III. RELAXATION TIME OF THE KURAMOTO ORDER PARAMETER

The level of synchronization in a general system $\mathcal{S}$ of $\mathcal{N}$ Kuramoto oscillators is described by a parameter r defined as

$$r(t)e^{i\psi(t)} = \frac{1}{\mathcal{N}}\sum_{x_n^\alpha\in\mathcal{S}} e^{i\theta_n^\alpha(t)} \to r(t) = \frac{1}{2N}\left|\sum_{x_n^\alpha\in\mathcal{M}} e^{i\theta_n^\alpha(t)}\right|, \quad (6)$$

where $\psi(t)$ is the average phase of the oscillators in the system. Here, $r \approx 1$ ($r \approx 0$) indicates a full synchronization (an asynchronous behavior) of the system $\mathcal{M}$ [33,34].

In this work, Eq. (6) is used to both layer (r^α) and global (r) order parameters by appropriately choosing the set of nodes (G^α or the whole set $\mathcal{M}$) where the sum is performed. The important issue regarding the definition of the α-layer order parameter (r^α) is to help understand the synchronization process at the α-layer level when interlayer coupling is changed. The global order parameter (r), which is common also to the plain monolayer Kuramoto model, does not provide a clear picture of the synchronization details by itself. $\psi^\alpha(t)$ and $\psi(t)$ indicate α-layer and multiplex average phases, respectively. When $M = 2$, it is possible to express r in terms r^α as

$$r = \sqrt{\frac{(r^1)^2 + (r^2)^2 + 2r^1r^2\cos(\psi^1 - \psi^2)}{4}}. \quad (7)$$

This can be easily obtained by multiplying $re^{i\psi}$ by $e^{-i\psi^2}$ and conducting the necessary manipulation.

For the purpose of putting forward the analytical results, we restrict our analysis to the $r^\alpha(t) \approx 1$ case, i.e., we assume that $\theta_n^\alpha(t) \approx \psi^\alpha(t)$ for $1 \leqslant n \leqslant N_\alpha$, $1 \leqslant \alpha \leqslant M$, $\forall\, t$. In Sec. IV we show that these conditions are fairly well satisfied for the system in Eq. (1) when, at $t = 0$, the degree of synchronization in each layer is high. Under such restrictions, we rewrite r for the $M = 2$ case as

$$r(t) \approx \left|\cos\left(\frac{\psi^1 - \psi^2}{2}\right)\right| = \left|\cos\left(\frac{\Delta}{2}\right)\right|, \quad (8)$$

where $\Delta(t) = \psi^1(t) - \psi^2(t)$ is the difference between the average phases of the layers G^1 and G^2. Hence, the time scales of r and $|\cos(\frac{\psi^1-\psi^2}{2})|$ are the same.

The linear relaxation time of the interlayer synchronization process can be estimated by the difference between the average phases of layers G^1 and G^2, Δ, defined in Eq. (8). Taking into account the property (i) of $S(\mathcal{L})$, the column eigenvector of Λ_Δ, $\vec{v}_\Delta$, is such that $\vec{v}_\Delta^T = (v_1^1,\ldots,v_N^1|v_1^2,\ldots,v_N^2) = (1,\ldots,1|-1,\ldots,-1)$.

By definition, $\mathbf{L}_1$ and $\mathbf{L}_2$ are symmetric real matrices with row and column sums zero, i.e., $\mathbf{L}_\alpha\vec{1} = \vec{0}$, where $\vec{x}$ is an all-x vector. Thus,

$$\mathcal{L}\vec{v}_\Delta = \left(\begin{array}{c|c}\lambda^1\mathbf{L}_1 & \mathbf{0}\\ \hline \mathbf{0} & \lambda^2\mathbf{L}_2\end{array}\right)\vec{v}_\Delta + \left(\begin{array}{c|c}\lambda^{12}\mathbf{I} & -\lambda^{12}\mathbf{I}\\ \hline -\lambda^{12}\mathbf{I} & \lambda^{12}\mathbf{I}\end{array}\right)\vec{v}_\Delta$$
$$= \vec{0} + 2\lambda^{12}\vec{v}_\Delta = \Lambda_\Delta\vec{v}_\Delta. \quad (9)$$

Following [43,48,49], the normal mode related to $\Lambda_\Delta = 2\lambda^{12}$ is

$$\vec{v}_\Delta^T\vec{\theta} = \sum_{x_n^1\in G^1}\theta_n^1 - \sum_{x_m^2\in G^2}\theta_m^2 = \varphi_\Delta(0)e^{-\Lambda_\Delta t}. \quad (10)$$

According to Eq. (8), when the assumption $r^\alpha(t) \approx 1$ is valid, Eq. (10) leads to

$$\Delta(t) = \psi^1(t) - \psi^2(t) \approx \frac{\varphi_\Delta(0)}{N}e^{-\Lambda_\Delta t}. \quad (11)$$

Since the relaxation time for interlayer synchronization can be estimated by $\tau_\Delta = 1/\Lambda_\Delta$, we draw the following similar conclusions to the results listed in Sec. II:

(i) When $\lambda^{12} \ll 1$, the diffusive time scale of $\mathcal{M}$ coincides with the interlayer synchronization time, i.e., $\Lambda_2 = \Lambda_\Delta$.

(ii) When $\lambda^{12} \gg 1$, the diffusive time scale of $\mathcal{M}$ exceeds the interlayer synchronization time, i.e., $\Lambda_2 \ll \Lambda_\Delta$ ($\Leftrightarrow \tau_\mathcal{M} \gg \tau_\Delta$).

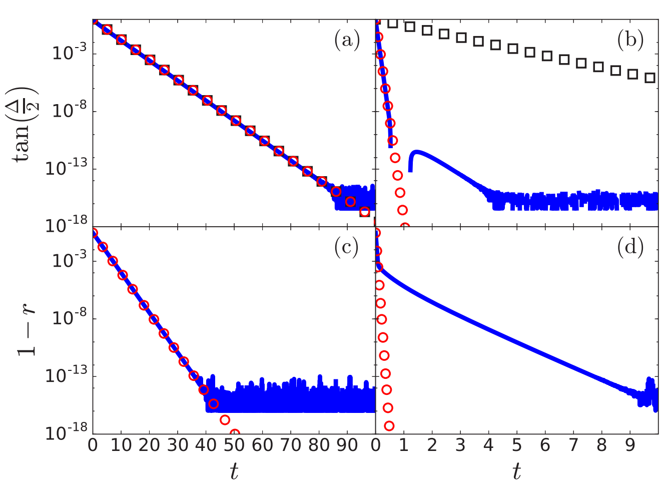

FIG. 3. Numerical results for $N = 500$, $\lambda = 2.0$, $\mu^1 = \pi/2$, $\mu^2 = 0$, and $a = 0.1$. Each multiplex layer has the same topological features described in Fig. 2. Panels (a) and (b): Time evolution of $\tan(\frac{\Delta(t)}{2})$ (blue continuous line), $\eta_\Delta(t)$ (red circles), and $\eta_2(t)$ (black squares) for $\lambda^{12} = 0.1\lambda$ (a) and $\lambda^{12} = 10.0\lambda$ (b). Panels (c) and (d): Time evolution of $1 - r(t)$ (blue continuous line) and $\eta_r(t)$ (red circles) for $\lambda^{12} = 0.1\lambda$ (c) and $\lambda^{12} = 10.0\lambda$ (d).

To derive the nonlinear relaxation time scale of the interlayer synchronization for the system in Eq. (1), we rewrite it in terms of the order parameters r^α of each layer G^α as

$$\dot{\theta}_n^\alpha = \Omega_n^\alpha + \lambda^\alpha r^\alpha N \bar{w}_n^\alpha \sin\left(\psi^\alpha - \theta_n^\alpha\right) + \sum_{\substack{\beta=1\\ \alpha\neq\beta}}^{M} \lambda^{\alpha\beta} w_{nn}^{\alpha\beta} \sin\left(\theta_n^\beta - \theta_n^\alpha\right), \tag{12}$$

where $\bar{w}_n^\alpha$ is defined by

$$\bar{w}_n^\alpha \sum_{x_m^\alpha \in G^\alpha} e^{i\theta_m^\alpha} = \sum_{x_m^\alpha \in G^\alpha} w_{nm}^\alpha e^{i\theta_m^\alpha}. \tag{13}$$

As $r^\alpha(t) \approx 1$, we obtain the following approximation for an undirected multiplex $\mathcal{M}$:

$$\dot{\psi}^\alpha = \frac{1}{N} \sum_{x_n^\alpha \in G^\alpha} \dot{\theta}_n^\alpha = \frac{1}{N}\left[\sum_{n=1}^{N} \Omega_n^\alpha\right] + \sum_{\substack{\beta=1\\ \alpha\neq\beta}}^{M} \lambda^{\alpha\beta} \sin(\psi^\beta - \psi^\alpha)\left[\sum_{n=1}^{N} w_{nn}^{\alpha\beta}\right] = \langle\Omega\rangle^\alpha + \sum_{\substack{\beta=1\\ \alpha\neq\beta}}^{M} \lambda^{\alpha\beta} \sin(\psi^\beta - \psi^\alpha)\frac{s^{\alpha\beta}}{N}, \tag{14}$$

where $s^{\alpha\beta}$ is the sum of the interlayer strengths between nodes of the layers G^α and G^β. Also, the evolution of the average phase difference between G^α and G^β becomes

$$\dot{\Delta}^{\alpha\beta} = \dot{\psi}^\alpha - \dot{\psi}^\beta = (\langle\Omega\rangle^\alpha - \langle\Omega\rangle^\beta) - 2\lambda^{\alpha\beta}\sin(\psi^\alpha - \psi^\beta)\frac{s^{\alpha\beta}}{N} + \sum_{\substack{\gamma=1\\ \gamma\neq\alpha,\beta}}^{M}\left[\lambda^{\alpha\gamma}\sin(\psi^\gamma - \psi^\alpha)\frac{s^{\alpha\gamma}}{N} - \lambda^{\beta\gamma}\sin(\psi^\gamma - \psi^\beta)\frac{s^{\beta\gamma}}{N}\right]. \tag{15}$$

Restricting the discussion to $M = 2$ and $w_{nn}^{12} = 1 \Rightarrow s^{12} = N$, we consider first $\langle\Omega\rangle^1 \approx \langle\Omega\rangle^2$, so that the synchronization of the system can be estimated as

$$\left|\tan\left(\frac{\Delta(t)}{2}\right)\right| \approx \left|\tan\left(\frac{\Delta(0)}{2}\right)\right| e^{-\int_0^t 2\lambda^{12} dt'} = \left|\tan\left(\frac{\Delta(0)}{2}\right)\right| e^{-\Lambda_\Delta t} \equiv \eta_\Delta(t), \tag{16}$$

where we use the short-hand notation $\Delta(t) = \Delta^{12}(t)$. Equation (16) and the series expansion $\tan(x) \simeq x$ show that the relaxation time of Δ is dominated by Λ_Δ, i.e., $\Delta/2 \propto e^{-\Lambda_\Delta t}$.

Next, if $\langle\Omega\rangle^1 \neq \langle\Omega\rangle^2$, it is possible to integrate Eq. (15) and express the corresponding solution in terms of a variable $\xi(t)$ such that

$$\xi(t) = \frac{\left|\tan\left(\frac{\Delta(t)}{2}\right) - \mathrm{sgn}(\langle\Omega\rangle^{12})(|R| - \sqrt{R^2-1})\right|}{\left|\tan\left(\frac{\Delta(t)}{2}\right) - \mathrm{sgn}(\langle\Omega\rangle^{12})(|R| + \sqrt{R^2-1})\right|} = \xi(0)e^{-t|\langle\Omega\rangle^{12}|\sqrt{R^2-1}}, \tag{17}$$

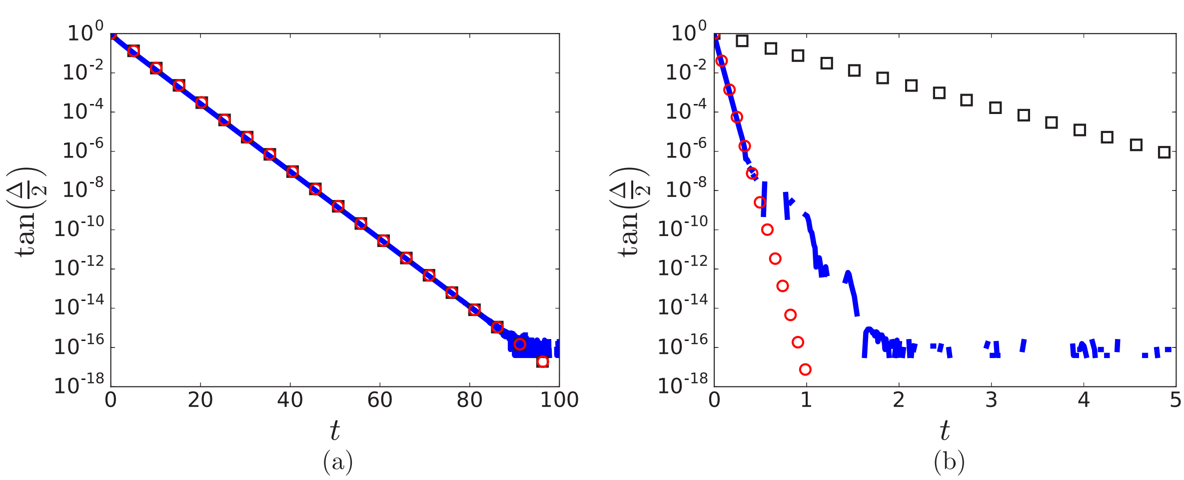

FIG. 4. Time evolution of $\tan\left(\frac{\Delta(t)}{2}\right)$, $\eta_\Delta(t)$, and $\eta_2(t)$ for $N = 50$, $\lambda = 2.0$, $\mu^1 = \pi/2$, $\mu^2 = 0$, and $a = 0.1$. Each layer contains an Erdös-Rényi random graph with mean degrees $\langle k\rangle = 4.04$ and 5.4, respectively. The used symbols and lines are the same as in Figs. 3(a) and 3(b). (a) Left panel: $\lambda^{12} = 0.1\lambda$. (b) Right panel: $\lambda^{12} = 10.0\lambda$.

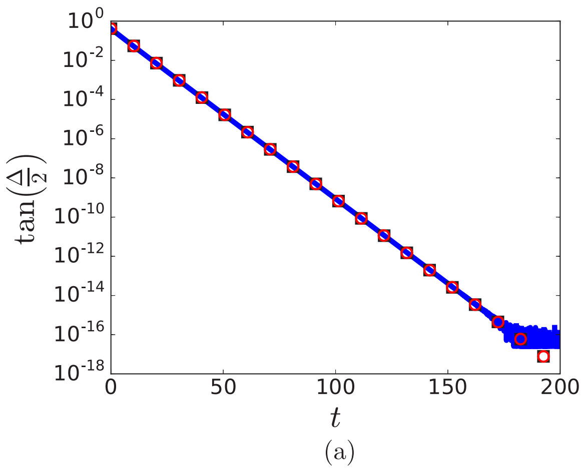

FIG. 5. Time evolution of $\tan(\frac{\Delta(t)}{2})$, $\eta_\Delta(t)$, and $\eta_2(t)$ for $N = 50$, $\lambda = 1.0$, $\mu^1 = \pi/4$, $\mu^2 = 0$, and $a = 0.01$. One layer contains an Erdös-Rényi random graph with mean degree $\langle k\rangle = 5.52$. The other one contains a network with asymptotic degree distribution $P(k) \sim k^{-3}$. The used symbols and lines are the same as in Figs. 3(a) and 3(b). (a) Left panel: $\lambda^{12} = 0.1\lambda$. (b) Right panel: $\lambda^{12} = 10.0\lambda$.

where sgn(·) is the sign function, $\langle\Omega\rangle^{12} \equiv \langle\Omega\rangle^1 - \langle\Omega\rangle^2$, and

$$R = \frac{\Lambda_\Delta}{\langle\Omega\rangle^1 - \langle\Omega\rangle^2} \equiv \frac{\Lambda_\Delta}{\langle\Omega\rangle^{12}}. \tag{18}$$

Equation (17) is valid when $|R| > 1$, while, for the $|R| \leqslant 1$, the integration of Eq. (15) results in

$$\tan\left(\frac{\Delta(t)}{2}\right) = R + \sqrt{1-R^2}\tan\left[\frac{\langle\Omega\rangle^{12}\sqrt{1-R^2}}{2}t + \tan^{-1}\left(\frac{\tan\left(\frac{\Delta(0)}{2}\right) - R}{\sqrt{1-R^2}}\right)\right]. \tag{19}$$

As can be observed, Eq. (19) shows that $\tan(\frac{\Delta(t)}{2})$ is a periodic function for $\Lambda_\Delta \leqslant |\langle\Omega\rangle^{12}|$. This drifting behavior just states that, if the interlayer coupling strength is not large enough, it is no longer possible to reduce the difference of the average frequencies between the layers and entrain the whole system.

Supposing that $\Delta/2 \gtrsim 0$, $\tan(\frac{\Delta(t)}{2}) \geqslant 2|R|$, and $\Lambda_\Delta \gg |\langle\Omega\rangle^{12}|$, the absolute value signs in Eq. (17) can be removed, thus it can be approximated as

$$\frac{\tan\left(\frac{\Delta}{2}\right)}{\tan\left(\frac{\Delta}{2}\right) - A} = -\frac{1}{A}\left(\frac{\Delta}{2}\right) - \frac{1}{A^2}\left(\frac{\Delta}{2}\right)^2 - \frac{(A^2+3)}{3A^3}\left(\frac{\Delta}{2}\right)^3 - \cdots \approx \xi(0)e^{-\Lambda_\Delta t}, \tag{20}$$

where $A = 2|R|\text{sgn}(\langle\Omega\rangle^{12})$. Under these conditions, the relaxation time of Δ is dominated once again by Λ_Δ. Hence, provided that $r^1(t) \approx r^2(t) \approx 1$ and $\Lambda_\Delta \gg |\langle\Omega\rangle^{12}|$, the nonlinear Kuramoto model [Eq. (1)] and the spectral analysis lead to the same relaxation time for the interlayer synchronization process for $M = 2$: $\tau_\Delta = 1/\Lambda_\Delta = 1/2\lambda^{12}$.

For small values of Δ, the time evolution of the order parameter in Eq. (8) can be approximated by $r(t) \simeq 1 - \Delta^2/8$. Therefore, the time scale of the order parameter (τ_r) is determined by the smallest nonzero power of $\Delta/2$, and a rough estimation is $\tau_r \gtrsim 1/2\Lambda_\Delta$.

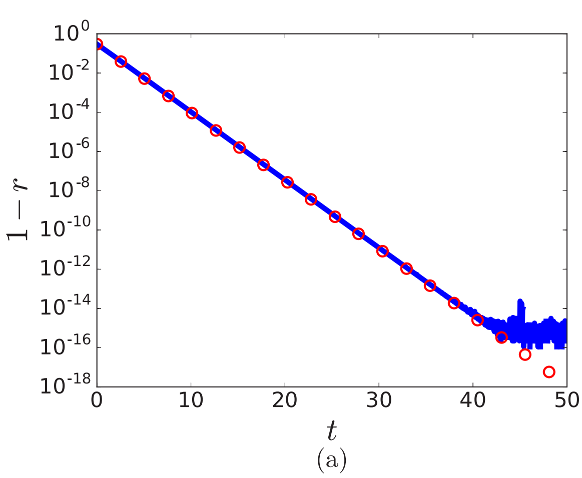

FIG. 6. Time evolution of $1 - r(t)$ and $\eta_r(t)$ for $N = 50$, $\lambda = 2.0$, $\mu^1 = \pi/2$, $\mu^2 = 0$, and $a = 0.1$. The used symbols and lines are the same as in Figs. 3(c) and 3(d). The multiplexes are the same as those used in Figs. 4(a) and 4(b). (a) Left panel: $\lambda^{12} = 0.1\lambda$. (b) Right panel: $\lambda^{12} = 10.0\lambda$.

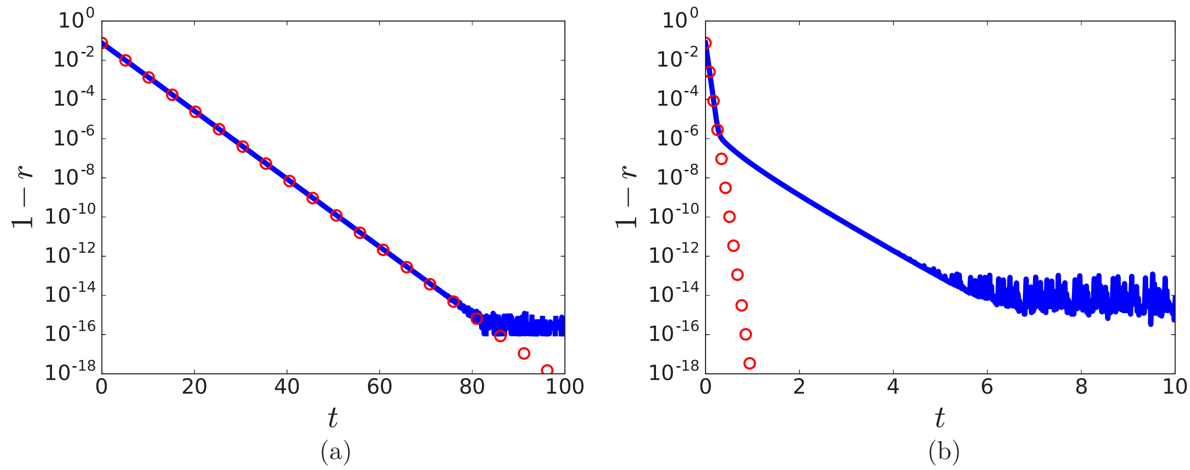

FIG. 7. Time evolution of $1-r(t)$ and $\eta_r(t)$. The used symbols and lines are the same as in Figs. 3(c) and 3(d). The multiplexes are the same as those used in Figs. 5(a) and 5(b). (a) Left panel: $\lambda^{12}=0.1\lambda$. (b) Right panel: $\lambda^{12}=10.0\lambda$.

Summarizing the results in Secs. II and III, the asymptotic synchronization phase of the Kuramoto model on multiplexes is characterized by the following behavior:

(i) When $\lambda^{12} \ll \lambda^1 = \lambda^2$, the time scales rank as follows: $\tau_{\mathcal{M}} = \tau_\Delta > \tau_r$.

(ii) When $\lambda^{12} \gg \lambda^1 = \lambda^2$, the time scales rank as follows: $\tau_{\mathcal{M}} \gg \tau_\Delta > \tau_r$.

According to Eq. (16), increasing the value of λ^{12} accelerates the transient regimes of the interlayer synchronization and of the global order parameter, respectively. Additionally, it reduces the difference between the average phase of each layer, and hence it favors the full synchronization of the system. Actually, it is important to call the attention to the fact that this result stays in opposition to what is observed for the multiplex diffusive relaxation when $r^\alpha \simeq 1$.

These results are in accordance with the prior findings on *superdiffusion* [5,43,45]. Superdiffusion emerges when the time scale of the multiplex is faster than that of both layers acting separately [5,43], i.e., $\Lambda_2 > \max(\sigma_2^1,\sigma_2^2)$, where σ_2^α is the smallest nonzero eigenvalue of the Laplacian matrix of layer G^α. For large coupling between layers, spectral analysis predicts that superdiffusion is not guaranteed; it depends on the specific structures coupled together. Increasing the interlayer coupling accelerates the convergence of the global order parameter and of the difference between the average phase of each layer. Nevertheless, it also increases the magnitude of the perturbations that are transmitted across the interlayer.

IV. NUMERICAL RESULTS

In this section, we show that the prior analytical findings are in complete agreement with computer simulations. We compare the results of the numerical integration of the coupled Kuramoto oscillators for several multiplexes realizations, using 16-digit variables. From the solution for $\theta_n^\alpha(t)$ we obtain the time evolution of $\tan\left(\frac{\Delta(t)}{2}\right)$ and $1-r(t)$ for the linear and nonlinear regimes that are compared, respectively, to

$$\eta_2(t) = \left|\tan\left(\frac{\Delta(0)}{2}\right)\right| e^{-\Lambda_2 t}, \quad \eta_r(t) = [1-r(0)]e^{-2\Lambda_\Delta t}. \tag{21}$$

$\eta_r(t)$ is a measure of the synchronization dynamics, while $\eta_2(t)$ has the same dependence on time as the multiplex diffusive dynamics. Besides that, $\tan\left(\frac{\Delta(t)}{2}\right)$ is also compared to $\eta_\Delta(t)$ in Eq. (16).

A. Linear Kuramoto model

We start by presenting numerical results from the integration of Eq. (2), where the initial phases $\theta_n^\alpha(0)$ are drawn randomly from a uniform distribution $\mathcal{U}_{\theta^\alpha}$ of width $2a$ centered at the value μ^α. Results satisfying $a \ll 1$ can be compared to the analytical expressions derived in the previous sections for $\tan\left(\frac{\Delta}{2}\right)$ and $1-r$, as in these cases the condition $r^\alpha \simeq 1$ is satisfied. For the sake of an easier comparison with the analytical results, we set $\lambda^1 = \lambda^2 = \lambda$. We remark that the results depend on the following factors: coupling strengths, initial conditions, and network topology.

The dependence on the coupling strengths is in agreement with Sec. III. Figure 3(a) [see also Figs. 4(a) and 5(a)] shows that, for $\lambda^{12} \ll \lambda$, the time scales of interlayer synchronization

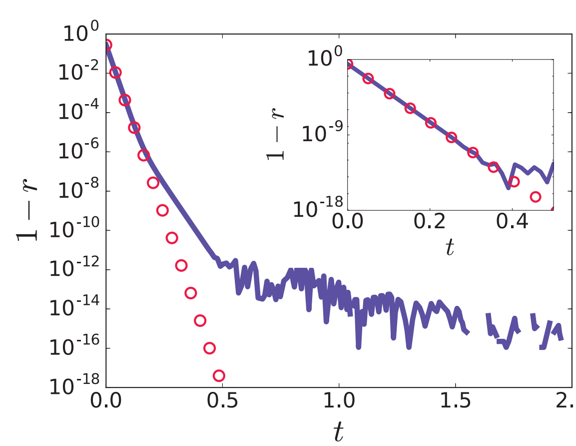

FIG. 8. Time evolution of $1-r(t)$ (blue continuous line) and $\eta_r(t)$ (red circles) for $N=10$, $\lambda=2.0$, $\lambda^{12}=10\lambda$, $\mu^1=\pi/2$, $\mu^2=0$, and $a=0.1$. Each layer contains a complete graph. The inset shows the results by considering $a=0$.

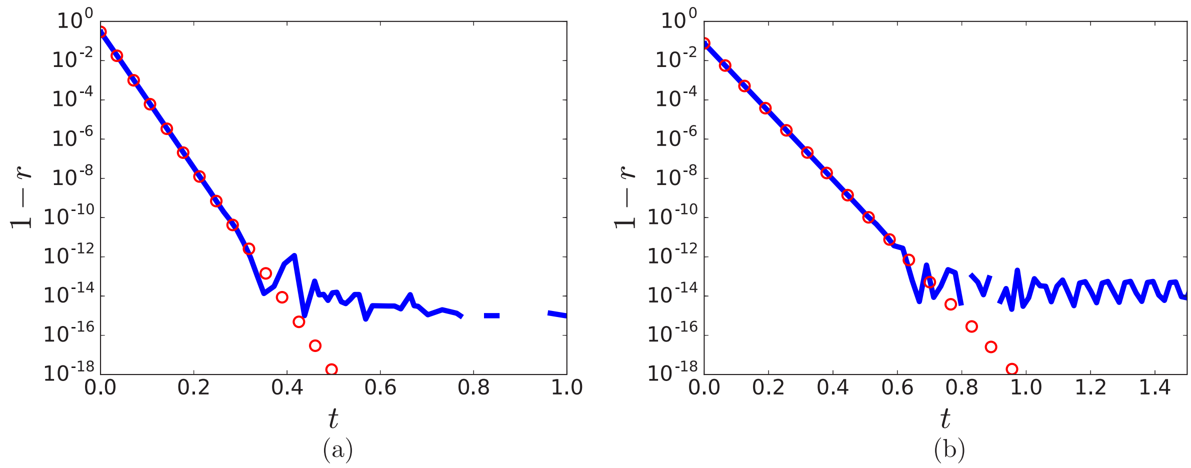

FIG. 9. Time evolution of $1 - r(t)$ and $\eta_r(t)$. $\lambda^{12} = 10\lambda$ in both panels, and the used symbols and lines are the same as in Fig. 8. (a) Left panel: The multiplexes are the same as those used in Figs. 4(a) and 4(b), except for $N = 15$ and $a = 0.0$. (b) Right panel: The multiplexes are the same as those used in Figs. 5(a) and 5(b), except for $a = 0.0$.

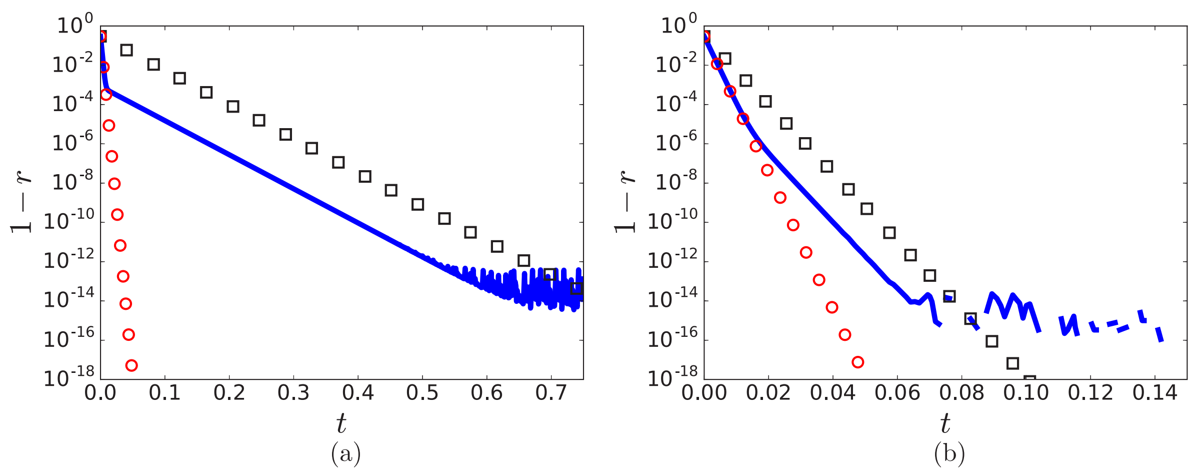

FIG. 10. Time evolution of $1 - r(t)$ (blue continuous line), $\eta_r(t)$ (red circles), and a guide for the eye proportional to $e^{-2\lambda N t}$ (black squares) for $\lambda = 2.0$, $\lambda^{12} = 100\lambda$, $\mu^1 = \pi/2$, $\mu^2 = 0$, and $a = 0.1$. Each layer contains a complete graph. (a) Left panel: $N = 10$. (b) Right panel: $N = 100$.

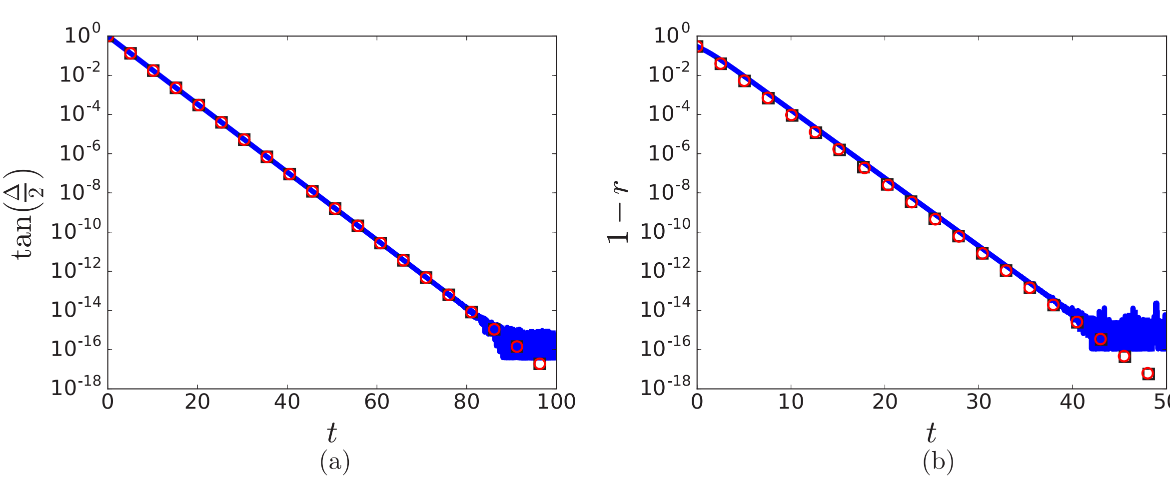

FIG. 11. (a) Left panel: Time evolution of $\tan\left(\frac{\Delta(t)}{2}\right)$, $\eta_\Delta(t)$, and $\eta_2(t)$. (b) Right panel: Time evolution of $1 - r(t)$ and $\eta_r(t)$. $\lambda^{12} = 0.1\lambda$ in both panels, and the used symbols and lines are the same as in Figs. 3(a) and 3(c). The multiplexes are the same as those used in Fig. 3.

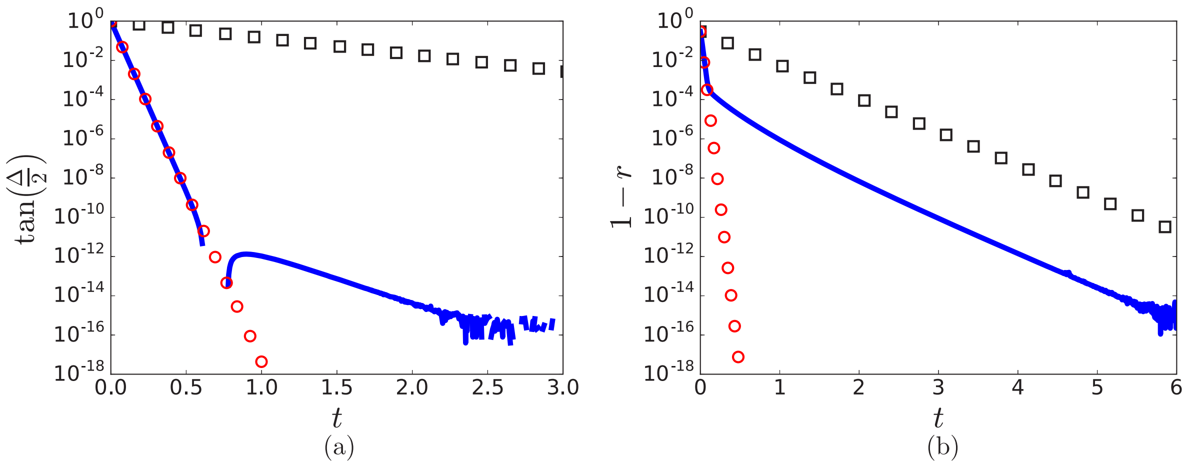

FIG. 12. (a) Left panel: Time evolution of $\tan(\frac{\Delta(t)}{2})$, $\eta_\Delta(t)$, and $\eta_2(t)$. (b) Right panel: Time evolution of $1 - r(t)$ and $\eta_r(t)$. $\lambda^{12} = 10.0\lambda$ in both panels, and the used symbols and lines are the same as in Figs. 3(b) and 3(d). The multiplexes are the same as those used in Fig. 3.

and of diffusion on $\mathcal{M}$ are equal: the time evolution of $\tan(\frac{\Delta(t)}{2})$ is well approximated by $\eta_\Delta(t)$ and $\eta_2(t)$, i.e., $\Lambda_2 \approx \Lambda_\Delta$. However, when $\lambda^{12} \gg \lambda$, these time scales differ, i.e., $\Lambda_2 \neq \Lambda_\Delta$, as indicated by lines with different slopes in Fig. 3(b) [see also Figs. 4(b) and 5(b)]. Moreover, it is also shown that the agreement between $\tan(\frac{\Delta(t)}{2})$ and $\eta_\Delta(t)$ has a lower limit $\sim 10^{-10}$. Nevertheless, the difference between the average phases of both layers relaxes faster than the whole system, i.e., $\tau_\mathcal{M} \gg \tau_\Delta$ for $\lambda \ll \lambda^{12}$. Both panels reveal the presence of random fluctuations $\sim 10^{-15}$, which depend on the precision of the used variables.

The same (somewhat different) features are observed in Figs. 3(c), 6(a) and 7(a) [Figs. 3(d), 6(b) and 7(b)], where we compare the approximation $\eta_r(t)$ with the actual value of $1 - r(t)$. The evolution of $1 - r(t)$ is well adjusted by $\eta_r(t)$ for $\lambda^{12} \ll \lambda$. However, when $\lambda^{12} \gg \lambda$, the quantities agree with each other in a more limited range $\gtrsim 10^{-4}$.

For a given choice of the coupling parameters, the deviations from the exponential behavior can be influenced by topological differences among the layers and by the initial values $\theta_n^\alpha(0)$. To emphasize the importance of the latter, we consider $M = 2$ multiplexes where each layer consists of a complete graph, for which analytical expressions for Λ_2 can be obtained (see the Appendix). In Fig. 8 we show the numerical results for $1 - r(t)$ when $a = 0$ and 0.1. The inset shows that the time evolution of $1 - r(t)$ is well adjusted by $\eta_r(t)$ when $a = 0$ [see also Figs. 9(a) and 9(b)], while departures from the exponential decay take place when $a > 0$. Here, the agreement between the curves is limited to the range $\gtrsim 10^{-6}$.

Figures 3 and 8 suggest that it may be possible to relate the range of values of $1 - r$ where the numerical results coincide with the analytical predictions to τ_D, the characteristic time scale for the emergence of these discrepancies. It turns out that τ_D is mainly controlled by the value of Λ_2 as follows:

$$\tau_D \approx \frac{1}{2\Lambda_2}. \tag{22}$$

Therefore, in the case $\Lambda_\Delta \approx \Lambda_2$, deviations disappear until the numeric precision of the used variables is reached, whether

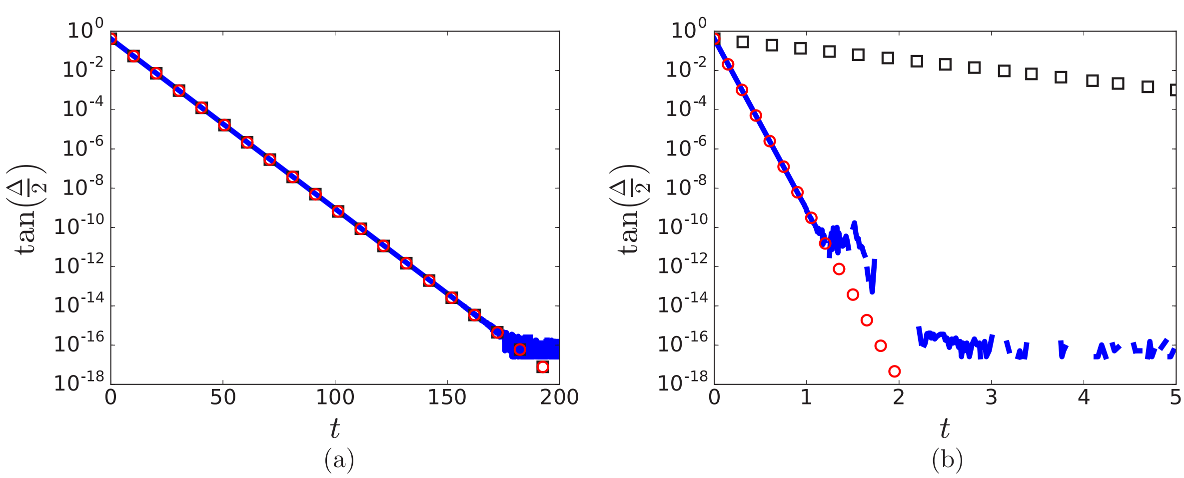

FIG. 13. Time evolution of $\tan(\frac{\Delta(t)}{2})$, $\eta_\Delta(t)$, and $\eta_2(t)$. $\Omega_n^\alpha = 0$ for all n in both panels, and the used symbols and lines are the same as in Figs. 3(a) and 3(b). The multiplexes are the same as those used in Figs. 5(a) and 5(b). (a) Left panel: $\lambda^{12} = 0.1\lambda$. (b) Right panel: $\lambda^{12} = 10.0\lambda$.

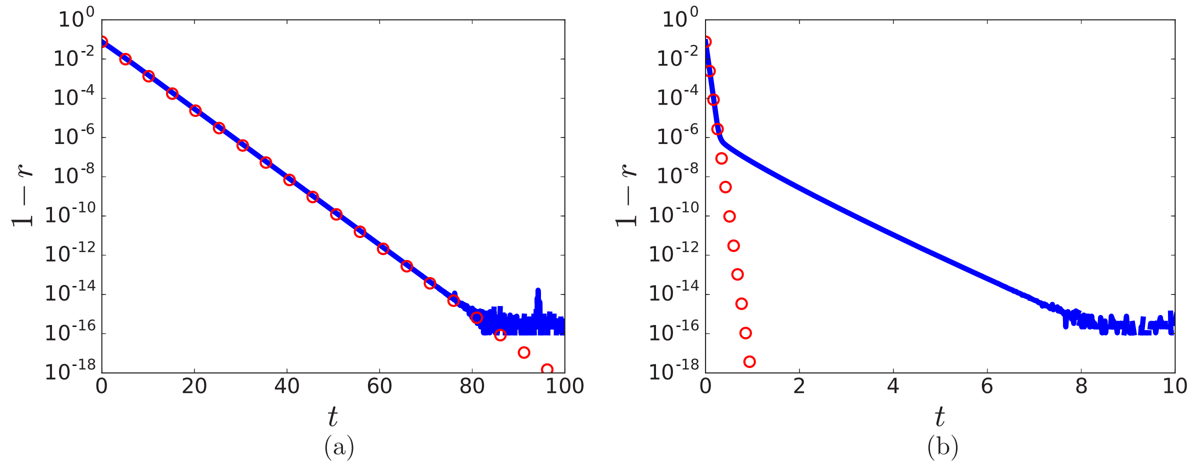

FIG. 14. Time evolution of $1 - r(t)$ and $\eta_r(t)$. $\Omega_n^\alpha = 0$ for all n in both panels, and the used symbols and lines are the same as in Figs. 3(c) and 3(d). The multiplexes are the same as those used in Figs. 5(a) and 5(b). (a) Left panel: $\lambda^{12} = 0.1\lambda$. (b) Right panel: $\lambda^{12} = 10.0\lambda$.

or not $a = 0$ [see Figs. 3(a), 3(c), 4(a) 5(a), 6(a), and 7(a)]. However, if $\Lambda_\Delta > \Lambda_2$ and $a > 0$, discrepancies will manifest.

Finally, still using complete graphs for the sake of comparison to analytical expressions, we illustrate the dependence of the multiplex dynamics on the topology for a given choice of the coupling strengths and the initial conditions. We note that the dependence on the topology can be observed just by changing the number of nodes in each layer of the complete graph. Indeed, if $\Lambda_\Delta > \Lambda_2$, the smallest nonzero eigenvalue of the supra-Laplacian matrix is $\Lambda_2 = \lambda N$ (see the Appendix). Therefore, according to Eq. (22), the smaller the number of nodes N, the larger are the deviations for $\tau_{\mathcal{M}} > \tau_\Delta$ and $a > 0$. In Figs. 10(a) and 10(b), we display the time evolution of $1 - r(t)$, $\eta_r(t)$, and a guide for the eye proportional to $e^{-2\lambda N t}$ for $N = 10$ and 100, respectively, and $a > 0$. As can be observed, these results are in good agreement with Eq. (22). In the Appendix, we show analytically the dependence of the global order parameter r on $e^{-2\Lambda_2 t}$ (i.e., $e^{-2\lambda N t}$), when each layer of the multiplex network is a complete graph.

B. Nonlinear Kuramoto model

The numerical results for the nonlinear equations (1) were obtained using the same procedure described in the previous subsection. When all natural frequencies of the oscillators are set to zero, i.e., $\Omega_n^\alpha = 0\ \forall n$, the time evolutions of $\tan\left(\frac{\Delta(t)}{2}\right)$ and $1 - r(t)$ for $\lambda^{12} \ll \lambda$ are essentially the same as those in Figs. 3(a) and 3(c) [see Figs. 11(a) and 11(b), respectively].

However, when $\lambda^{12} \gg \lambda$, which causes $\Lambda_2 \neq \Lambda_\Delta$ and $\tau_{\mathcal{M}} \gg \tau_\Delta$, $\tan\left(\frac{\Delta(t)}{2}\right)$ deviates from both $\eta_2(t)$ and $\eta_\Delta(t)$, and $1 - r(t)$ deviates from $\eta_r(t)$. The comparison between Figs. 3(b) and 12(a) shows that the nonlinear terms affect the evolution $\tan\left(\frac{\Delta(t)}{2}\right)$. Notice that the effect on the evolution of $1 - r(t) \sim \Delta^2$ is much smaller, in such a way that the changes induced by the nonlinear terms in Fig. 12(b) are minute in comparison to Fig. 3(d).

Other examples for different values of the interlayer and intralayer coupling constants and several initial conditions for the coupled Kuramoto oscillators are presented in Figs. 13(a),

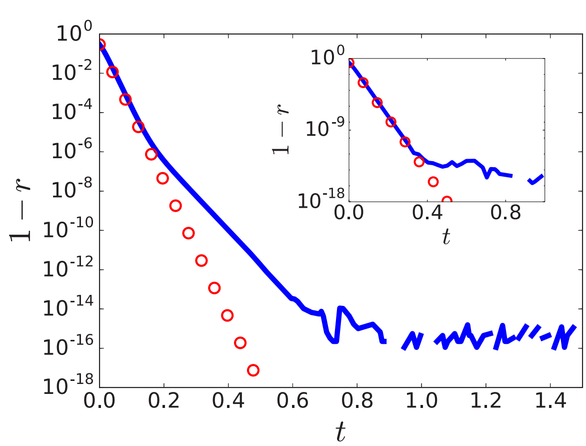

FIG. 15. Time evolution of $1 - r(t)$ (blue continuous line) and $\eta_r(t)$ (red circles) for $N = 10$, $\lambda = 2.0$, $\lambda^{12} = 10\lambda$, $\mu^1 = \pi/2$, $\mu^2 = 0$, and $a = 0.1$. Each layer contains a complete graph. The inset shows $a = 0$.

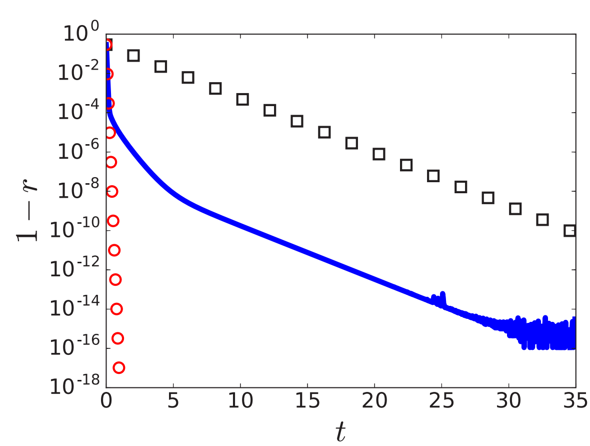

FIG. 16. Time evolution of $1 - r(t)$ (blue continuous line), $\eta_r(t)$ (red circles), and a guide for the eye proportional to $e^{-2\Lambda_2 t}$ (black squares). $\lambda^{12} = 10\lambda$ and $\Omega_n^\alpha = 0$. The multiplex is the same as those used in Figs. 4(a) and 4(b), except for $N = 15$ and $\lambda = 1.0$.

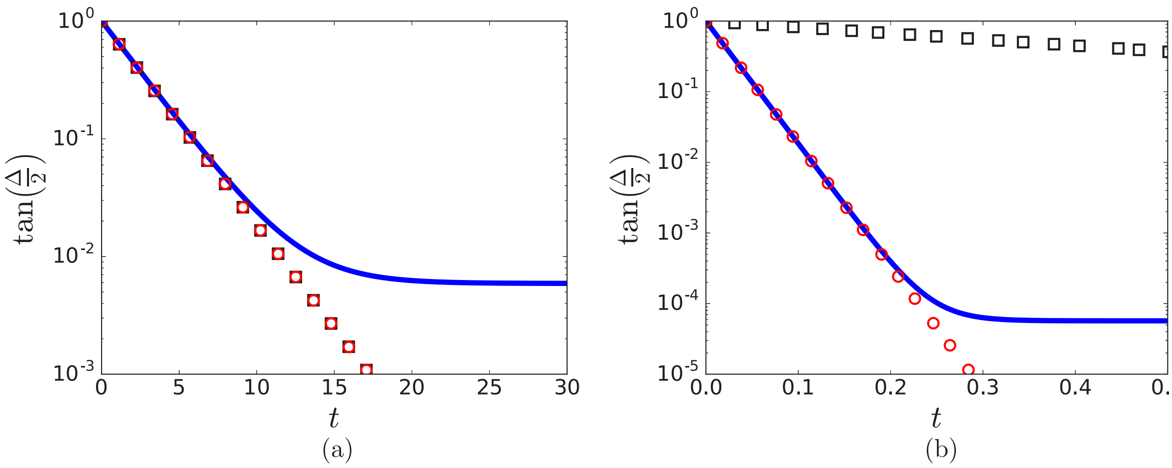

FIG. 17. Time evolution of $\tan\left(\frac{\Delta(t)}{2}\right)$, $\eta_\Delta(t)$, and $\eta_2(t)$. The multiplex parameters, symbols, and lines are the same as in Figs. 3(a) and 3(b), except for $\Omega_n^\alpha \in \mathcal{U}(0.8,1.2)$. (a) Left panel: $\lambda^{12} = 0.1\lambda$. (b) Right panel: $\lambda^{12} = 10.0\lambda$.

13(b), 14(a), and 14(b). All of them are in complete agreement with the results described in this section.

The dependence of $1 - r(t)$ on a for $M = 2$ multiplexes formed by complete graphs is very similar to that in Fig. 8. When $a = 0$, $1 - r(t)$ and $\eta_r(t)$ are in complete agreement if they are greater than or similar to 10^{-12}, while for $a = 0.1$, deviations appear when $\eta_r(t) \lesssim 10^{-5}$ (see Figs. 15 and 16).

Let us now discuss the results when the natural frequencies Ω_n^α are different from zero so that, in general, $\langle\Omega\rangle^1 \neq \langle\Omega\rangle^2$. Following [54], the values of the frequencies are drawn randomly from a uniform distribution $\mathcal{U}(0.8,1.2)$. As observed in Figs. 17(a) and 17(b), the time evolution of $\tan\left(\frac{\Delta(t)}{2}\right)$ diverges from $\eta_\Delta(t)$ when $\langle\Omega\rangle^1 \neq \langle\Omega\rangle^2$ for both $\lambda^{12} \ll \lambda$ and $\lambda^{12} \gg \lambda$. In both cases, Δ converges to a nonzero value and, consequently, the oscillators do not reach full synchronization in accordance with Eqs. (17) and (18). We notice that the deviations from the exponential predictions for $\lambda^{12} \ll \lambda$ occur at a larger value of $\eta_2(t)$ as compared to $\lambda^{12} \ll \lambda$. This stays in opposition to the previously observed behavior for $\Omega_n^\alpha \equiv 0$. Indeed, a relatively small interlayer coupling favors the emergence of the deviations once interlayer synchronization is impeded for $\lambda^{12} \approx 0$. Hence, if $|\langle\Omega\rangle^{12}| > 0$ and $\lambda^{12} \approx 0$, the exponential decay barely takes place. In the case of $\lambda^{12} \gg 0$, the relaxation time of the synchronization error gets closer to the estimation given by $\eta_r(t)$ whether or not $\lambda \gg \lambda^{12}$.

The asymptotic value of the difference between the average phases of both layers can be estimated from Eq. (17). If $\tan\left(\frac{\Delta(t)}{2}\right) \geqslant \mathrm{sgn}(\langle\Omega\rangle^{12})(|R| + \sqrt{R^2 - 1})$, Eq. (17) can be rewritten as

$$\tan\left(\frac{\Delta(t)}{2}\right) = \left(|R| - \sqrt{R^2 - 1}\,\frac{1 + \xi(0)e^{-t|\langle\Omega\rangle^{12}|\sqrt{R^2-1}}}{1 - \xi(0)e^{-t|\langle\Omega\rangle^{12}|\sqrt{R^2-1}}}\right) \times \mathrm{sgn}(\langle\Omega\rangle^{12}), \tag{23}$$

so that its asymptotic value $t \to \infty$ is given by

$$\lim_{t\to\infty} \tan\left(\frac{\Delta(t)}{2}\right) = (|R| - \sqrt{R^2 - 1})\mathrm{sgn}(\langle\Omega\rangle^{12}). \tag{24}$$

If $\langle\Omega\rangle^1 \simeq \langle\Omega\rangle^2$, R diverges and Δ decays to zero exponentially. On the other hand, in Fig. 18 we expose the time evolution of $\tan\left(\frac{\Delta(t)}{2}\right)$ for $2\langle\Omega\rangle^{12} = \Lambda_\Delta$. In that case, according to Eqs. (17) and (24), the asymptotic value of the difference between the average phases of both layers is $\psi^1 - \psi^2 = \pi/6$ (green triangles). It is easy to see that the prior estimation is very accurate. Other examples for different conditions are presented in Figs. 19(a) and 19(b). All of them are in complete agreement with the results described in this section.

Figures 20(a) and 21(a) [Figs. 20(b) and 21(b)] illustrate the behavior of $1 - r(t)$ for small (large) interlayer coupling, respectively. As can be observed, synchronization error departs from $\eta_r(t)$ values whether or not $\lambda^{12} \ll \lambda$. As expected, its asymptotic value does not decay to zero.

Finally, we show that $\Delta(t)$ is a periodic function in the case of $\Lambda_\Delta \leqslant |\langle\Omega\rangle^{12}|$ (see Fig. 22). As can be observed, its time evolution is in complete agreement with that obtained from Eq. (19).

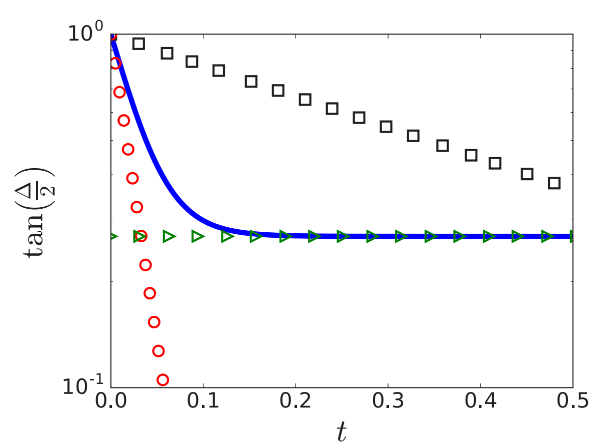

FIG. 18. Time evolution of $\tan\left(\frac{\Delta(t)}{2}\right)$, $\eta_\Delta(t)$, and $\eta_2(t)$. The multiplex parameters, symbols, and lines are the same as in Fig. 3(b). The model parameters are $\lambda = 2.0$, $\lambda^{12} = 10\lambda$, and $2\langle\Omega\rangle^{12} = \Lambda_\Delta$. Green triangles indicate the asymptotic value obtained with Eq. (17).

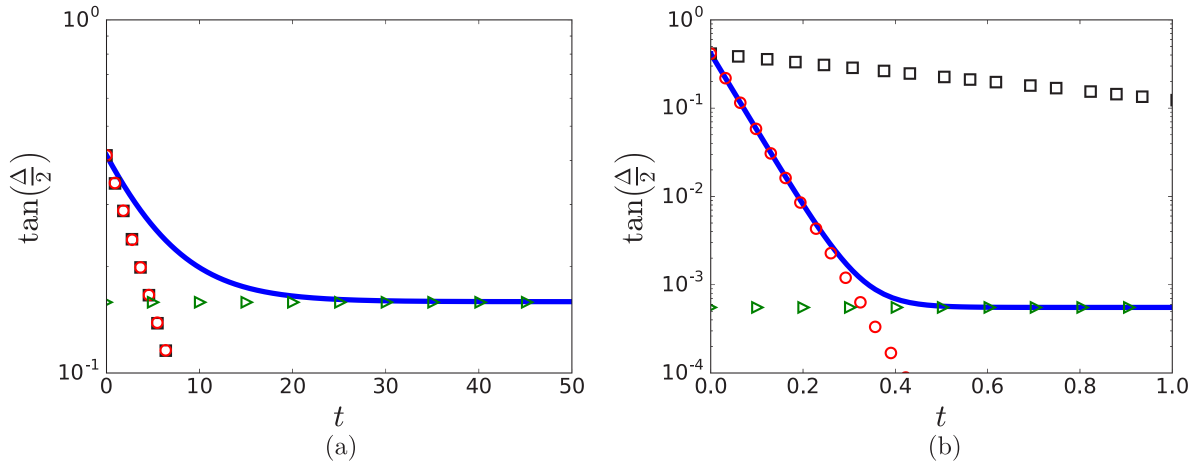

FIG. 19. Time evolution of $\tan\left(\frac{\Delta(t)}{2}\right)$, $\eta_{\Delta}(t)$, and $\eta_2(t)$. The used symbols and lines are the same as in Fig. 18. The multiplex parameters are the same as those used in Figs. 5(a) and 5(b), except for $\Omega_n^{\alpha} \in \mathcal{U}(0.8,1.2)$ for all n. (a) Left panel: $\lambda^{12} = 0.1\lambda$. (b) Right panel: $\lambda^{12} = 10.0\lambda$.

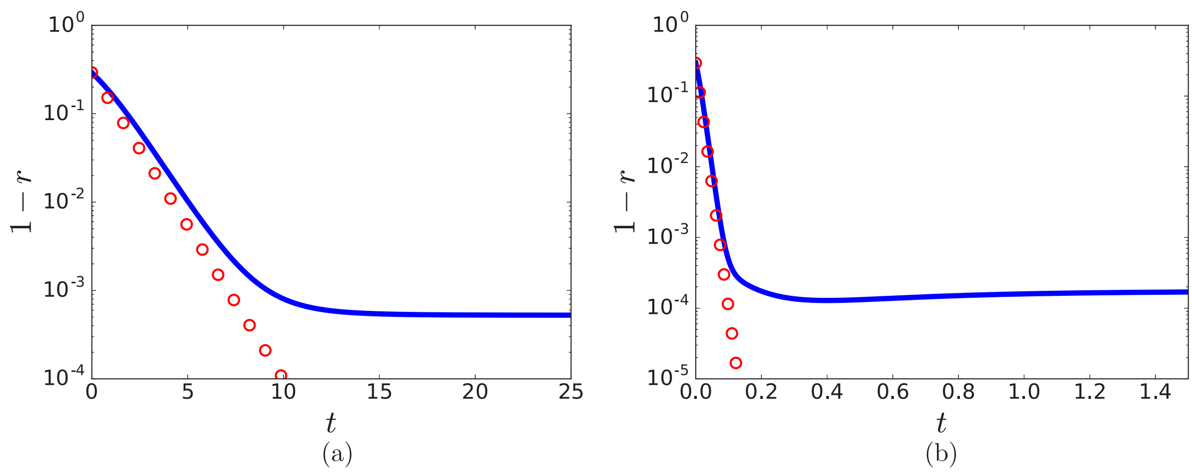

FIG. 20. Time evolution of $1 - r(t)$ and $\eta_r(t)$. The multiplex parameters, symbols, and lines are the same as in Figs. 3(c) and 3(d), except for $\Omega_n^{\alpha} \in \mathcal{U}(0.8,1.2)$. (a) Left panel: $\lambda^{12} = 0.1\lambda$. (b) Right panel: $\lambda^{12} = 10.0\lambda$.

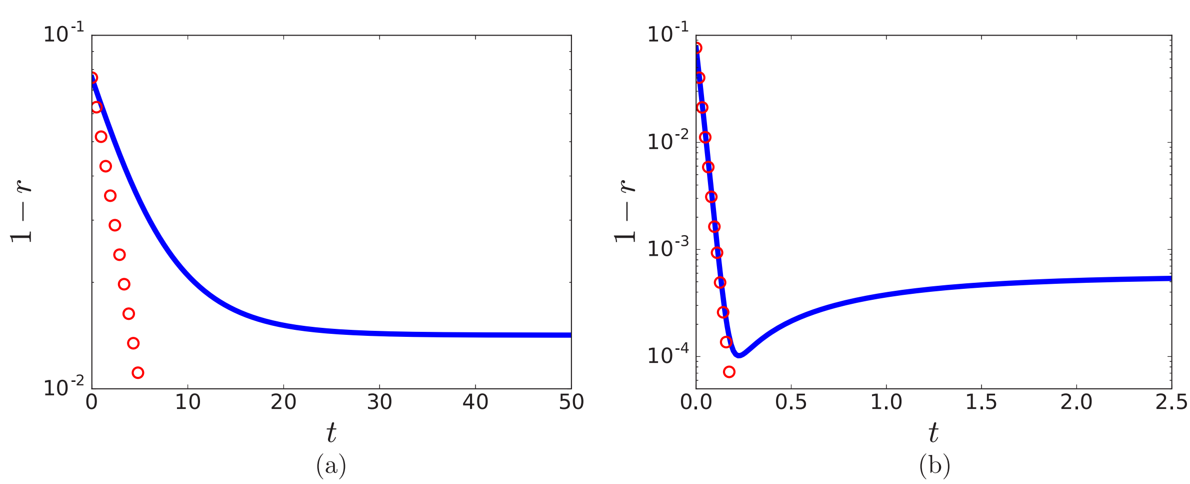

FIG. 21. Time evolution of $1 - r(t)$ and $\eta_r(t)$. The used symbols and lines are the same as in Figs. 20(a) and 20(b). The multiplex parameters are the same as those used in Figs. 5(a) and 5(b), except for $\Omega_n^{\alpha} \in \mathcal{U}(0.8,1.2)$ for all n. (a) Left panel: $\lambda^{12} = 0.1\lambda$. (b) Right panel: $\lambda^{12} = 10.0\lambda$.

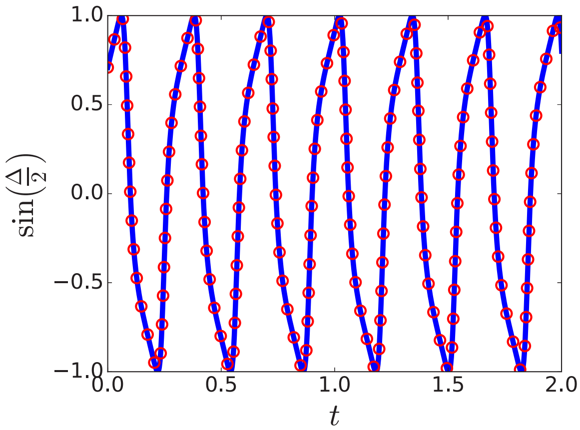

FIG. 22. Time evolution of $\sin(\frac{\Delta(t)}{2})$ (blue continuous line) and the results adapted from Eq. (19) (red circles) for $N = 500$, $\lambda = 2.0$, $\lambda^{12} = 10\lambda$, $\mu_1 = \pi/2$, $\mu_2 = 0$, $a = 0.1$, and $2.8\Lambda_\Delta = |\langle\Omega\rangle^{12}|$. The multiplex parameters are the same as those used in Fig. 3.

V. CONCLUSIONS

We have developed a simple formalism to study the time scales of the global order parameter and the interlayer synchronization of multilayer networks. Our approach has been adapted to a two-layer multiplex with high degrees of synchronization in each layer [i.e., $r^\alpha(t) \approx 1$ for $1 \leqslant \alpha \leqslant 2$ and $t \geqslant 0$] in a particular setup in which nodes are preserved through layers.

We have analyzed the difference between the average phase of each layer of the multiplex network from two different perspectives: spectral analysis and the nonlinear Kuramoto model. Our analytical results showed that the time scales of the global order parameter τ_r and the interlayer synchronization τ_Δ are inversely proportional to the interlayer coupling strength λ^{12}. Surprisingly, the convergence of the global order parameter is faster than the convergence of interlayer synchronization, and the latter is generally faster than the relaxation time of the multiplex network $\tau_{\mathcal{M}}$. These features do not depend on the specific structures coupled together. Therefore, increasing the interlayer coupling always shortens the global order parameter and the interlayer synchronization transient regimes.

On the other hand, our formalism outlined the effects of frequencies on the evolution of the global order parameter and on the interlayer synchronization process. In addition, conditions for an oscillatory behavior were also identified.

The analytical findings were in fairly good agreement with computer simulations. In the case of multiplex networks with relatively small interlayer coupling (i.e., $\lambda^{12} \ll \lambda$), similar average frequencies in each layer (i.e., $\langle\Omega\rangle^1 \approx \langle\Omega\rangle^2$), and high degrees of synchronization in each layer at the initial time (i.e., $r^\alpha(0) \approx 1$ for $1 \leqslant \alpha \leqslant 2$), the analytical and numerical results were in complete agreement. However, supposing similar average frequencies in each layer, if the interlayer coupling is relatively large (i.e., $\lambda^{12} \gg \lambda$), and if there exists an initial intralayer phase heterogeneity (i.e., there is at least one layer G^α that contains two or more oscillators whose phases are different at $t = 0$), the numerical results show deviations from the predicted exponential decay, although major changes of the global order parameter and of the interlayer synchronization were fairly well adjusted by our analytical approach. The time scale of these discrepancies, τ_D, is inversely proportional to $2\Lambda_2$, where Λ_2 is the smallest nonzero eigenvalue of the supra-Laplacian matrix $\mathcal{L}$ of the multiplex network. According to prior works [5,43], this dependence on Λ_2 implies that deviations from our analytical results are shaped by topological characteristics of the layers involved as well as the respective values of λ and λ^{12}.

When the average frequencies of each layer are dissimilar (i.e., $\langle\Omega\rangle^{12} = \langle\Omega\rangle^1 - \langle\Omega\rangle^2 \neq 0$), computer simulations are in good agreement with our analytical results. If $\Lambda_\Delta \geqslant |\langle\Omega\rangle^{12}|$, the asymptotic values of the global order parameter and of the interlayer synchronization converge to a nonzero value. If $\Lambda_\Delta \leqslant |\langle\Omega\rangle^{12}|$, a periodic behavior is obtained. Discrepancies from our analytical description do not appear unless the asymptotic values of the global order parameter and of the interlayer synchronization are close to zero (i.e., $\langle\Omega\rangle^{12} \approx 0$).

Thus, under the hypotheses of this work, we conclude that the time scale of the global order parameter is at least twice as small as the time scale of multiplex networks (i.e., $2\tau_r \approx 2\tau_D \approx \tau_{\mathcal{M}} = 1/\Lambda_2$), and the major changes of this parameter are fairly well adjusted by our analytical findings (i.e., $\tau_r \approx \tau_\Delta = 1/\Lambda_\Delta = 1/2\lambda^{12}$).

ACKNOWLEDGMENTS

This work was supported by the project MTM2015-63914-P from the Ministry of Economy and Competitiveness of Spain and by the Brazilian agency CNPq (Grant No. 305060/2015-5). R.F.S.A. also acknowledges the support of the National Institute of Science and Technology for Complex Systems (INCT-SC Brazil).

APPENDIX: ANALYTICAL RESULTS FOR A MULTIPLEX NETWORK FORMED BY COMPLETE GRAPHS

1. Eigenvalue spectrum of the supra-Laplacian matrix

Given an undirected multiplex network $\mathcal{M}$ with $M = 2$ layers, if both layers contain a complete network, then the supra-Laplacian matrix $\mathcal{L}$ has the following eigenvalues Λ:

(i) $\Lambda = 0$. It is a nondegenerate eigenvalue.

(ii) $\Lambda = \lambda N$. It is a degenerate eigenvalue. It appears $N - 1$ times.

(iii) $\Lambda = 2\lambda^{12}$. It is a nondegenerate eigenvalue.

(iv) $\Lambda = 2\lambda^{12} + \lambda N$. It is a degenerate eigenvalue. It appears $N - 1$ times.

Thus, in the case of $\lambda^{12}/\lambda \geqslant N/2$ ($\lambda^{12}/\lambda < N/2$), the smallest nonzero eigenvalue of the supra-Laplacian matrix is $\Lambda = \lambda N$ ($\Lambda = 2\lambda^{12}$).

2. Estimation of the average time evolution of the linear Kuramoto model

Given an undirected multiplex network $\mathcal{M}$ with $M = 2$ layers, if both layers contain a complete network, then Eq. (2) results in

$$\dot{\theta}_n^\alpha(t) = \lambda^\alpha N\langle\theta^\alpha\rangle - \lambda^\alpha N\theta_n^\alpha + \lambda^{12}\big(\theta_n^\beta - \theta_n^\alpha\big), \tag{A1}$$

where

$$\langle\theta^\alpha\rangle = \frac{1}{N}\sum_{x_n^\alpha\in G^\alpha}\theta_n^\alpha. \quad \text{(A2)}$$

We estimate the average value of $\dot{\theta}_n^\alpha$ in the layer G^α, $\langle\dot{\theta}^\alpha\rangle$. The result is given by

$$\langle\dot{\theta}^\alpha\rangle = \frac{1}{N}\sum_{n=1}^{N}\dot{\theta}_n^\alpha = -\lambda^{12}(\langle\theta^\alpha\rangle - \langle\theta^\beta\rangle). \quad \text{(A3)}$$

Note that according to Eq. (A3), the sum of the phases of the multiplex network is constant, for $M = 2$, when each layer contains a complete graph, i.e., $\langle\dot{\theta}^1\rangle + \langle\dot{\theta}^2\rangle = 0$. Therefore,

$$\langle\theta^1(t)\rangle + \langle\theta^2(t)\rangle = \langle\theta^1(0)\rangle + \langle\theta^2(0)\rangle = \Gamma. \quad \text{(A4)}$$

On the other hand, according to Eq. (A3), it can be written that

$$\langle\dot{\theta}^1\rangle - \langle\dot{\theta}^2\rangle = -2\lambda^{12}(\langle\theta^1\rangle - \langle\theta^2\rangle). \quad \text{(A5)}$$

It results in

$$\langle\theta^1(t)\rangle - \langle\theta^2(t)\rangle = [\langle\theta^1(0)\rangle - \langle\theta^2(0)\rangle]e^{-2\lambda^{12}t} = \gamma e^{-2\lambda^{12}t}. \quad \text{(A6)}$$

Hence, the evolutions of the average value of θ^1 and of the average value of θ^2 are given by

$$\langle\theta^1(t)\rangle = \frac{\gamma}{2}e^{-2\lambda^{12}t} + \frac{\Gamma}{2} \quad \text{(A7)}$$

and

$$\langle\theta^2(t)\rangle = -\frac{\gamma}{2}e^{-2\lambda^{12}t} + \frac{\Gamma}{2}. \quad \text{(A8)}$$

By considering the series expansion,

$$e^{i\theta_n^\alpha} = e^{i\langle\theta^\alpha\rangle} + ie^{i\langle\theta^\alpha\rangle}\left(\theta_n^\alpha - \langle\theta^\alpha\rangle\right) - \tfrac{1}{2}e^{i\langle\theta^\alpha\rangle}\left(\theta_n^\alpha - \langle\theta^\alpha\rangle\right)^2 + \cdots, \quad \text{(A9)}$$

we observe that

$$\sum_{x_n^\alpha\in G\alpha} e^{i\theta_n^\alpha} = Ne^{i\langle\theta^\alpha\rangle} + ie^{i\langle\theta^\alpha\rangle}\left(\left[\sum_{x_n^\alpha\in G\alpha}\theta_n^\alpha\right] - N\langle\theta^\alpha\rangle\right) - \frac{1}{2}e^{i\langle\theta^\alpha\rangle}\left(\left[\sum_{x_n^\alpha\in G\alpha}\left(\theta_n^\alpha\right)^2\right] + N\langle\theta^\alpha\rangle^2 - 2\langle\theta^\alpha\rangle\sum_{x_n^\alpha\in G\alpha}\theta_n^\alpha\right) + \cdots$$
$$\approx Ne^{i\langle\theta^\alpha\rangle} - \frac{1}{2}e^{i\langle\theta^\alpha\rangle}[N\langle(\theta^\alpha)^2\rangle + N\langle\theta^\alpha\rangle^2 - 2N\langle\theta^\alpha\rangle^2]. \quad \text{(A10)}$$

We characterize the degree of synchronization of each layer G^α by means of its own order parameter, r^α, expressed by

$$r^\alpha(t)e^{i\psi^\alpha(t)} = \frac{1}{N}\sum_{x_n^\alpha\in G^\alpha} e^{i\theta_n^\alpha(t)} \rightarrow r^\alpha(t) = \frac{1}{N}\left|\sum_{x_n^\alpha\in G^\alpha} e^{i\theta_n^\alpha(t)}\right|. \quad \text{(A11)}$$

Consequently, according to Eqs. (A10) and (A11), it is straightforward to realize that $\psi^\alpha \approx \langle\theta^\alpha\rangle$ and

$$r^\alpha \approx 1 + \tfrac{1}{2}\langle\theta^\alpha\rangle^2 - \tfrac{1}{2}\langle(\theta^\alpha)^2\rangle. \quad \text{(A12)}$$

In the case $M = 2$, we obtain the following expressions for $\langle(\theta^1)^2\rangle$, $\langle(\theta^2)^2\rangle$, and $\langle\theta^1\theta^2\rangle$, respectively:

$$\langle(\theta^1)^2\rangle = \frac{\Gamma^2}{4} + K_1e^{-2\lambda Nt} + \frac{\gamma^2}{4}e^{-4\lambda^{12}t} - K_2e^{-2(\lambda N+2\lambda^{12})t} + \frac{\gamma\Gamma}{2}e^{-2\lambda^{12}t} + K_3e^{-(2\lambda N+2\lambda^{12})t}, \quad \text{(A13)}$$

$$\langle(\theta^2)^2\rangle = \frac{\Gamma^2}{4} + K_1e^{-2\lambda Nt} + \frac{\gamma^2}{4}e^{-4\lambda^{12}t} - K_2e^{-2(\lambda N+2\lambda^{12})t} - \frac{\gamma\Gamma}{2}e^{-2\lambda^{12}t} - K_3e^{-(2\lambda N+2\lambda^{12})t}, \quad \text{(A14)}$$

and

$$\langle\theta^1\theta^2\rangle = \frac{\Gamma^2}{4} + K_1e^{-2\lambda Nt} - \frac{\gamma^2}{4}e^{-4\lambda^{12}t} + K_2e^{-2(\lambda N+2\lambda^{12})t}, \quad \text{(A15)}$$

where K_1, K_2, and K_3 are constant values that depend on the initial conditions, given by

$$K_1 = \frac{2\langle\theta^1\theta^2\rangle(0) - \Gamma^2 + \langle(\theta^1)^2\rangle(0) + \langle(\theta^2)^2\rangle(0)}{4}, \quad \text{(A16)}$$

$$K_2 = \frac{2\langle\theta^1\theta^2\rangle(0) + \gamma^2 - \langle(\theta^1)^2\rangle(0) - \langle(\theta^2)^2\rangle(0)}{4}, \quad \text{(A17)}$$

and

$$K_3 = \frac{\langle(\theta^1)^2\rangle(0) - \langle(\theta^2)^2\rangle(0) - \gamma\Gamma}{2}. \quad \text{(A18)}$$

Thus, according to Eqs. (A7), (A8), (A13), and (A14), the order parameters for layers G^1 and G^2 are given by

$$r^1 \approx 1 - \tfrac{1}{2}K_1e^{-2\lambda Nt} + \tfrac{1}{2}K_2e^{-2(\lambda N+2\lambda^{12})t} - \tfrac{1}{2}K_3e^{-(2\lambda N+2\lambda^{12})t} = \zeta - \chi \quad \text{(A19)}$$

and

$$r^2 \approx 1 - \tfrac{1}{2}K_1e^{-2\lambda Nt} + \tfrac{1}{2}K_2e^{-2(\lambda N+2\lambda^{12})t} + \tfrac{1}{2}K_3e^{-(2\lambda N+2\lambda^{12})t} = \zeta + \chi, \quad \text{(A20)}$$

where

$$\zeta = \left(e^{2\lambda Nt} - \tfrac{1}{2}K_1 - \tfrac{1}{2}K_2e^{-4\lambda^{12}t}\right)e^{-2\lambda Nt} \quad \text{(A21)}$$

and

$$\chi = \tfrac{1}{2}K_3e^{-2\lambda^{12}t}e^{-2\lambda Nt}. \quad \text{(A22)}$$

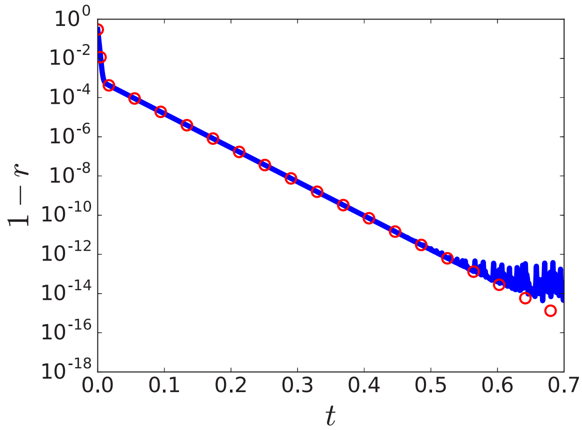

FIG. 23. Time evolution of $1 - r(t)$ (blue continuous line) and the results obtained with Eq. (A23) (red circles) for $N = 10$, $\lambda = 2.0$, $\lambda^{12} = 100\lambda$, $\mu_1 = \pi/2$, $\mu_2 = 0$, and $a = 0.1$. Each layer contains a complete graph.

Finally, the global order parameter of the multiplex network $\mathcal{M}$ [given by Eq. (7)] can be approximated as

$$r = \sqrt{\frac{(r^1)^2 + (r^2)^2 + 2r^1r^2\cos(\Delta)}{4}} \approx \sqrt{\zeta^2\cos^2\left(\frac{\Delta}{2}\right) + \chi^2\sin^2\left(\frac{\Delta}{2}\right)}, \tag{A23}$$

where

$$\Delta = \psi^1 - \psi^2 \approx \langle\theta^1\rangle - \langle\theta^2\rangle = \gamma e^{-2\lambda^{12}t}. \tag{A24}$$

In Fig. 23, we compare the numerical results for $1 - r(t)$ with the estimation obtained from Eq. (A23) when $\Lambda_\Delta \gg \Lambda$ (i.e., $2\lambda^{12} \gg N\lambda$) and there exists an initial intralayer phase heterogeneity ($a > 0$). As can be observed, they are in good agreement.

[1] S. Boccaletti, G. Bianconi, R. Criado, C. I. D. Genio, J. Gómez-Gardeñes, M. Romance, I. Sendiña-Nadal, Z. Wang, and M. Zanin, The structure and dynamics of multilayer networks, Phys. Rep. **544**, 1 (2014).
[2] M. Kivelä, A. Arenas, M. Barthelemy, J. P. Gleeson, Y. Moreno, and M. A. Porter, Multilayer networks, J. Complex Netw. **2**, 203 (2014).
[3] S. V. Buldyrev, R. Parshani, G. Paul, H. Eugene Stanley, and S. Havlin, Catastrophic cascade of failures in interdependent networks, Nature (London) **464**, 1025 (2010).
[4] F. R. K. Chung, *Spectral Graph Theory* (American Mathematical Society, Philadelphia, 1997), Vol. 92.
[5] A. Solé-Ribalta, M. De Domenico, N. E. Kouvaris, A. Díaz-Guilera, S. Gómez, and A. Arenas, Spectral properties of the Laplacian of multiplex networks, Phys. Rev. E **88**, 032807 (2013).
[6] R. Parshani, S. V. Buldyrev, and S. Havlin, Interdependent Networks: Reducing the Coupling Strength Leads to a Change from a First to Second Order Percolation Transition, Phys. Rev. Lett. **105**, 048701 (2010).
[7] J. F. Donges, H. C. H. Schultz, N. Marwan, Y. Zou, and J. Kurths, Investigating the topology of interacting networks, Eur. Phys. J. B **84**, 635 (2011).
[8] J. Gao, S. V. Buldyrev, H. E. Stanley, and S. Havlin, Networks formed from interdependent networks, Nat. Phys. **8**, 40 (2012).
[9] F. Battiston, V. Nicosia, and V. Latora, Structural measures for multiplex networks, Phys. Rev. E **89**, 032804 (2014).
[10] L. Solá, M. Romance, R. Criado, J. Flores, A. G. D. Amo, and S. Boccaletti, Eigenvector centrality of nodes in multiplex networks, Chaos **23**, 033131 (2013).
[11] M. De Domenico, A. Solé-Ribalta, E. Cozzo, M. Kivelä, Y. Moreno, M. A. Porter, S. Gómez, and A. Arenas, Mathematical Formulation of Multilayer Networks, Phys. Rev. X **3**, 041022 (2013).
[12] A. Cardillo, J. Gómez-Gardeñes, M. Zanin, M. Romance, D. Papo, F. D. Pozo, and S. Boccaletti, Emergence of network features from multiplexity, Sci. Rep. **3**, 1344 (2013).
[13] A. Cardillo, M. Zanin, J. Gómez-Gardeñes, M. Romance, A. G. D. Amo, and S. Bocaletti, Modeling the multi-layer nature of the european air transport network: Resilience and passengers re-scheduling under random failures, Eur. J. Spec. Top. **215**, 23 (2013).
[14] M. Szell, R. Lambiotte, and S. Thurner, Multirelational organization of large-scale social networks in an online world, Proc. Natl. Acad. Sci. USA **107**, 13636 (2010).
[15] R. Gallotti and M. Barthelemy, Anatomy and efficiency of urban multimodal mobility, Sci. Rep. **4**, 6911 (2014).
[16] R. Gallotti, M. Porter, and M. Barthelemy, Lost in transportation: Information measures and cognitive limits in multilayer navigation, Sci. Adv. **2**, e1500445 (2016).
[17] L. Lotero, R. Hurtado, L. M. Floría, and J. Gómez-Gardeñes, Rich do not rise early: Spatio-temporal patterns in the mobility networks of different socio-economic classes, R. Soc. Open Sci. **3**, 150654 (2016).
[18] F. Radicchi and A. Arenas, Abrupt transition in the structural formation of interconnected networks, Nat. Phys. **9**, 717 (2013).
[19] J. Gómez-Gardeñes, M. De Domenico, G. Gutiérrez, A. Arenas, and S. Gómez, Layer-layer competition in multiplex complex networks, Philos. Trans. R. Soc. A **373**, 20150117 (2015).
[20] J. Gómez-Gardeñes, I. Reinares, A. Arenas, and L. M. Floría, Evolution of cooperation in multiplex networks, Sci. Rep. **2**, 620 (2012).
[21] J. T. Matamalas, J. Poncela-Casasnovas, and A. Arenas, Strategic incoherence regulates cooperation in social dilemmas on multiplex networks, Sci. Rep. **5**, 9519 (2015).
[22] Z. Wang, A. Szolnoki, and M. Perc, Evolution of public cooperation on interdependent networks: The impact of biased utility functions, Europhys. Lett. **97**, 48001 (2012).
[23] Z. Wang, L. Wang, and M. Perc, Degree mixing in multilayer networks impedes the evolution of cooperation, Phys. Rev. E **89**, 052813 (2014).
[24] F. Sorrentino, Synchronization of hypernetworks of coupled dynamical systems, New J. Phys. **14**, 033035 (2012).

[25] L. V. Gambuzza, M. Frasca, and J. Gómez-Gardeñes, Intra-layer synchronization in multiplex networks, Europhys. Lett. **110**, 20010 (2015).
[26] R. Sevilla-Escoboza, R. Gutiérrez, G. Huerta-Cuellar, S. Boccaletti, J. Gómez-Gardeñes, A. Arenas, and J. M. Buldú, Enhancing the stability of the synchronization of multivariable coupled oscillators, Phys. Rev. E **92**, 032804 (2015).
[27] C. I. D. Genio, J. Gómez-Gardeñes, I. Bonamassa, and S. Boccaletti, Synchronization in networks with multiple interaction layers, Sci. Adv. **2**, e1601679 (2016).
[28] M. S. Baptista, R. M. Szmoski, R. F. Pereira, and S. E. de S. Pinto, Chaotic, informational and synchronous behavior of multiplex networks, Sci. Rep. **6**, 22617 (2016).
[29] S. K. Dwivedi, M. S. Baptista, and S. Jalan, Optimization of synchronizability in multiplex networks by rewiring one layer, Phys. Rev. E **95**, 040301 (2017).
[30] N. E. Kouvaris, S. Hata, and A. Díaz- Guilera, Pattern formation in multiplex networks, Sci. Rep. **5**, 10840 (2015).
[31] M. Asllani, D. M. Busiello, T. Carletti, D. Fanelli, and G. Planchon, Turing patterns in multiplex networks, Phys. Rev. E **90**, 042814 (2014).
[32] C. Granell, S. Gómez, and A. Arenas, Dynamical Interplay Between Awareness and Epidemic Spreading in Multiplex Networks, Phys. Rev. Lett. **111**, 128701 (2013).
[33] Y. Kuramoto, in *Self-Entrainment of a Population of Coupled Non-linear Oscillators*, edited by H. Araki, Lecture Notes in Physics (Springer, Berlin, 1975).
[34] Y. Kuramoto, *Chemical Oscillations, Waves, and Turbulence* (Springer, Berlin, 1984).
[35] S. H. Strogatz, *Sync: The Emerging Science of Spontaneous Order* (Hyperion, New York, 2003).
[36] S. C. Manrubia, *Emergence of Dynamical Order: Synchronization Phenomena in Complex Systems* (World Scientific, Singapore, 2004).
[37] D. Kelly and G. A. Gottwald, On the topology of synchrony optimized networks of a kuramoto-model with non-identical oscillators, Chaos **21**, 025110 (2011).
[38] J. A. Acebrón, L. L. Bonilla, C. J. P. Vicente, F. Ritort, and R. Spigler, The kuramoto model: A simple paradigm for synchronization phenomena, Rev. Mod. Phys. **77**, 137 (2005).
[39] F. A. Rodrigues, T. K. DM. Peron, P. Ji, and J. Kurths, The kuramoto model in complex networks, Phys. Rep. **610**, 1 (2016).
[40] E. Ott and T. M. Antonsen, Low dimensional behavior of large systems of globally coupled oscillators, Chaos **18**, 037113 (2008).
[41] E. Barreto, B. Hunt, E. Ott, and P. So, Synchronization in networks of networks: The onset of coherent collective behavior in systems of interacting populations of heterogeneous oscillators, Phys. Rev. E **77**, 036107 (2008).
[42] D. Anderson, A. Tenzer, G. Barlev, M. Girvan, T. M. Antonsen, and E. Ott, Multiscale dynamics in communities of phase oscillators, Chaos **22**, 013102 (2012).
[43] S. Gomez, A. Diaz-Guilera, J. Gomez-Gardeñes, C. J. Perez-Vicente, Y. Moreno, and A. Arenas, Diffusion Dynamics on Multiplex Networks, Phys. Rev. Lett. **110**, 028701 (2013).
[44] M. De Domenico, M. A. Porter, and A. Arenas, Muxviz: A tool for multilayer analysis and visualization of networks, J. Complex Netw. **3**, 159 (2015).
[45] A. B. Serrano, J. Gómez-Gardeñes, and R. F. S. Andrade, Optimizing diffusion in multiplexes by maximizing layer dissimilarity, Phys. Rev. E **95**, 052312 (2017).
[46] K. M. Lee, B. Min, and K. I. Goh, Towards real-world complexity: An introduction to multiplex networks, Eur. Phys. J. B **88**, 48 (2015).
[47] M. De Domenico, C. Granell, M A. Porter, and A. Arenas, The physics of spreading processes in multilayer networks, Nat. Phys. **12**, 901 (2016).
[48] A. Arenas, A. Díaz-Guilera, and C. J. Pérez-Vicente, Synchronization Reveals Topological Scales in Complex Networks, Phys. Rev. Lett. **96**, 114102 (2006).
[49] A. Arenas, A. Díaz-Guilera, and C. J. Pérez-Vicente, Synchronization processes in complex networks, Physica D **224**, 27 (2006).
[50] J. A. Almendral and A. Díaz-Guilera, Dynamical and spectral properties of complex networks, New J. Phys. **9**, 187 (2007).
[51] C. Grabow, S. Grosskinsky, and M. Timme, Speed of complex network synchronization, Eur. Phys. J. B **84**, 613 (2011).
[52] C. Grabow, S. Hill, S. Grosskinsky, and M. Timme, Do small worlds synchronize fastest? Europhys. Lett. **90**, 48002 (2010).
[53] S.-W. Son, H. Jeong, and H. Hong, Relaxation of synchronization on complex networks, Phys. Rev. E **78**, 016106 (2008).
[54] V. Avalos-Gaytán, J. A. Almendral, D. Papo, S. E. Schaeffer, and S. Boccaletti, Assortative and modular networks are shaped by adaptive synchronization processes, Phys. Rev. E **86**, 015101 (2012).